

1 Article

2 Optimization of Reaction Selectivity Using CFD- 3 Based Compartmental Modeling and Surrogate- 4 Based Optimization

5 Shu Yang, San Kiang, Parham Farzan and Marianthi Ierapetritou*

6 Department of Chemical and Biochemical Engineering, Rutgers, The State University of New Jersey, 98
7 Brett Road, Piscataway, NJ 08854, USA ; yang.shu.public@gmail.com (S.Y.); san.kiang@gmail.com (S.K.);
8 parhamfarzan@gmail.com (P.F.); marianth@soe.rutgers.edu (M.I.)

9 * Correspondence: marianth@soe.rutgers.edu; Tel.: +1-848-445-2971

10

11 **Abstract:** Mixing is considered as a critical process parameter (CPP) during process development
12 due to its significant influence on reaction selectivity and process safety. Nevertheless, mixing issues
13 are difficult to identify and solve owing to their complexity and dependence on knowledge of
14 kinetics and hydrodynamics. In this paper, we proposed an optimization methodology using
15 Computational Fluid Dynamics (CFD) based compartmental modelling to improve mixing and
16 reaction selectivity. More importantly, we have demonstrated that through the implementation of
17 surrogate-based optimization, the proposed methodology can be used as a computationally non-
18 intensive way for rapid process development of reaction unit operations. For illustration purpose,
19 reaction selectivity of a process with Bourne competitive reaction network is discussed. Results
20 demonstrate that we can improve reaction selectivity by dynamically controlling rates and locations
21 of feeding in the reactor. The proposed methodology incorporates mechanistic understanding of the
22 reaction kinetics together with an efficient optimization algorithm to determine the optimal process
23 operation and thus can serve as a tool for quality-by-design (QbD) during product development
24 stage.

25 **Keywords:** mixing; CFD-simulation; surrogate-based optimization; compartmental modeling;
26 competing reaction system; optimization; model order reduction

27

28 1. Introduction

29 In chemical synthesis, many important reactions can be accompanied by undesired side-
30 reactions. This leads to wastes and affects product quality. Therefore, incorporating knowledge of
31 mixing can substantially improve reaction selectivity and yield, in addition to enhancing process
32 safety. Furthermore, due to a growing variety of reactors, characterization of mixing has become vital
33 in process development [1, 2]. To achieve optimal selectivity and yield, appropriate modeling of the
34 mass transport process in reactors is critical [3]. Nevertheless, owing to the complexity of mass
35 transport in turbulent flow, analyzing mixing remains a difficult problem.

36 Frequently, mixing in reactor is approximated by residence time distribution (RTD) analysis,
37 where residence time is experimentally measured through a tracer test. This approximation has been
38 proved to work relatively well, however “*RTD is not a complete description of structure for a
39 particular reactor or system of reactors*” [3]. Therefore, when reaction with high conversion rates
40 are considered, analysis solely based on RTD can lead to significant error [4]. Based on local sensors,
41 RTD characterization of tracer test can be improved by mixing time measurement [5, 6]. However,
42 considering potential bias and the requirement for specific equipment for tracer tests, RTD and
43 mixing time measurement have become less preferable comparing to the more resource-effective
44 benchmark reaction method [7]. Therefore, competitive reaction systems have become the standard

45 for mixing analysis [7-9]. Among the competitive reaction systems, the “*well-documented and*
46 *highly reliable*” [7] Bourne reaction and Villiermaux reaction is most commonly adopted [10]. The
47 mentioned systems of competitive reactions are based on the pioneering framework proposed by the
48 group of Bourne [11]. It has been proved that mixing can influence not only the reaction rate, but also
49 the distribution of products [12]. In Bourne’s framework, product distribution of competitive
50 reactions is analyzed to characterize mixing inhomogeneity inside reactors. Two most commonly
51 used categories of reactions have been proposed based on this framework: the neutralization and
52 alkaline hydrolysis of ester [13], and the iodide/iodate reaction scheme [14].

53 With rapid advances in computer technology, computational fluid dynamics (CFD) has become
54 a powerful tool to studying mixing. Comparing with the experimental methods, it provides detailed
55 understanding of mixing phenomenon in a timely-efficient manner without requiring meticulous
56 choice of equipment and sensors. In reaction engineering, CFD has been employed to study mixing
57 in chemical reactors [15-19], and bio-reactors [20-22], where good agreement with experiments were
58 achieved. The complex hydrodynamics, mass transfer, heat transfer and reaction kinetic can be
59 satisfactorily captured by CFD, making it a powerful tool in process design. Nonetheless, despite the
60 growing computational resources available, CFD still requires considerable computational time.

61 Despite the extensive study of mixing in different systems, owing to the resource and time
62 expense of experiments and CFD simulations, incorporating detailed understanding of mixing in
63 process operation optimization remains challenging. Even though CFD has been used to
64 systematically optimize reactor designs [23-26], optimization of process operations based on
65 dynamics of mixing remains complicated. For the past decade, research in mixing have started to
66 incorporate detailed knowledge of mixing from CFD to computationally inexpensive compartmental
67 models [20, 27-29], which has shown great potential for modeling mixing. Nevertheless, since space
68 is discrete in compartmental model, efficient optimization algorithm should be implemented to deal
69 with the complexity introduced by integer variables.

70 In this work, a modeling and optimization methodology is developed that systematically
71 improves reaction selectivity through optimized process operation and offers a more general
72 framework for improving reaction selectivity with a numerically efficient Quality-by-Design (QbD)
73 tool. In a case study, Bourne reaction is employed as a benchmark, which serve as a more explicit
74 quantification for the efficiency of mixing. It has been demonstrated in this work that CFD-based
75 compartmental model can be an efficient alternative for CFD simulations. By integrating CFD-based
76 compartmental model with surrogate-based optimization, the proposed framework has shown a
77 great potential for fast process development.

78 **2. Integrating CFD-based compartmental model with surrogate based optimization**

79 This section presents the development and implementation of the proposed methodology.
80 Initially, a detail description of flow field in the reactor is generated by a CFD simulation. It should
81 be noted that in stirred tank reactors the flow field are considered independent from chemical
82 reactions. As a result, the fluid dynamics data can be used for different reactions, which could
83 contribute to rapid process design and cost reduction. The result from CFD simulation is used to
84 develop a compartmental model, which would be discussed in subsections 2.1. Comparing to direct
85 CFD simulation, computational complexity of compartmental model is significantly reduced.
86 Therefore, the optimal process design can be determined numerically without prohibitive
87 computational expense. The process selectivity is then optimized by integrating the compartmental
88 model with surrogate-based optimization, as will be discussed in subsection 2.2.

89 *2.1. CFD-based compartmental model*

90 *2.1.1. A brief review of compartmental model*

91 Compartmental model defines a matrix of perfectly mixed control volumes interconnected by
92 the exchanging mass flux. In this method the reactors are discretized into a set of homogeneous
93 control volumes according to the defined mesh. The volume-averaged variable in all control volumes

94 are solved together to represent the space distribution inside the reactor. Compartmental modeling
 95 was regarded as a crude tool to study transport process and only provide basic understandings [30].
 96 However, by incorporating detailed CFD simulation to compartmental model, substantial
 97 improvement can be achieved leading to satisfactory agreement with experimental data without loss
 98 of computational efficiency [29, 31].

99 Considering the excessive computational and economical expense usually required by CFD
 100 simulation, for CMC development, CFD-based compartmental model have been adopted as
 101 computationally cheaper alternative [4, 27, 31-33] In addition to the reduced computational expense,
 102 CFD-based compartmental model provides the required simplifications for development work.
 103 Unlike CFD, which is not widely available and requires special know-how, CFD-based
 104 compartmental model can be easily implemented for different reaction systems based on flow field
 105 data determined beforehand. Adjustment in chemical kinetics do not usually require extra CFD
 106 simulation, which could save time and reduce cost.

107 In this proposed methodology, compartmental model is developed from CFD simulation based
 108 on the idea outlined by Bezzo et al [27]. Two key steps are required for model construction: (1)
 109 Topological mapping between two models through aggregating CFD cells into compartments. (2)
 110 Quantifying mass flux between different compartments. Topology mapping between CFD and
 111 compartmental model can be done either manually or automatically. Manual allocation of CFD cells
 112 is based on preliminary knowledge of flow field, which can be conducted prior to CFD simulation
 113 [20, 29, 34, 35]. Automatic mapping, on the other hand, merges computational cells based on CFD
 114 simulation to form meaningful homogeneous control volumes [4, 36]. Manual allocation usually
 115 leads to simpler mesh structure, which allow for efficient implementation of optimization tools.
 116 Therefore, in this work manual allocation is conducted, as will be outlined in subsection 2.1.3.

117 2.1.2. Compartmental model development

118 Mixing of particles inside the reactor is described by Eq.1, where C_i is the concentration of
 119 species i , N_i represents the mass flux of species i , and R_i denotes the source of species i .
 120 Compartmental models are obtained by volume averaging Eq.1 over each predefined compartment
 121 V , as described in Eq.2.

$$\frac{\partial C_i}{\partial t} = -\nabla \cdot \mathbf{N}_i + R_i, \quad (1)$$

$$\frac{d}{dx} \int_V \bar{C}_i dV = - \int_V \nabla \cdot \mathbf{N}_i dV + \int_V R_i dV, \quad (2)$$

122 Adopting the divergence theorem and replacing C_i with the volume-averaged concentration
 123 \bar{C}_{i,K_j} , Eq.2 is modified to Eq.3, where V_j is the volume of control volume K_j , and S_j is the surface of
 124 control volume K_j . The mass flux \mathbf{N} consist of convection and diffusion, where the diffusion is
 125 modelled by Fick's law with diffusion coefficient D . The source term R_i models the homogeneous
 126 consumption and generation of species i , which include chemical reactions and micro mixing. Due to
 127 the assumption of homogeneous compartments, the volume integral of source term in Eq.5
 128 is modified as follows:

$$V_j \frac{d\bar{C}_{i,K_j}}{dx} + \oint_{S_j} \mathbf{N}_{i,K_j} \cdot \mathbf{n} dS = \int_{K_j} R_i dV, \quad (3)$$

$$V_j \frac{d\bar{C}_{i,K_j}}{dx} = - \int_{S_j} \mathbf{v} \cdot \bar{C}_{i,K_j} \cdot \mathbf{n} dS + \int_{S_j} D \cdot \nabla C \cdot \mathbf{n} dS + \int_{K_j} R_i dV, \quad (4)$$

$$\int_{K_j} R_i dV = V_j \cdot R_{i,K_j}, \quad (5)$$

129 It should be recognized that the homogeneous assumption depends upon the Damköhler
 130 number (Da) in each compartment, which is a strong function of grid size, as will be discussed in
 131 subsection 2.1.3. Moreover, in this work diffusion mass transfer between different compartments
 132 are neglected, which is also justified in subsection 2.1.3 based on an analysis of the Péclet number

133 (Pe). The dominance of convective mass transfer would simplify Eq.4 into Eq.6, where Q_{jk} denotes
134 the flow rate from control volume j to control volume k .

$$V_j \frac{d\overline{C_{i,K_j}}}{dt} = -\overline{C_{i,K_j}} \sum_k Q_{j,k} + \sum_l (Q_{l,j} \cdot \overline{C_{i,K_l}}) + V_j \cdot R_{i,K_j}, \quad (6)$$

135 From CFD simulation, mass flow rate Q between different compartments can be easily calculated
136 through the topology mapping and merging strategy as mentioned in subsection 2.1.2. As a result,
137 the computational complexity of CFD is reduced while preserving the accurate flow pattern
138 description. For illustration purposes, a well-known pair of parallel competitive Bourne reactions is
139 studied. As will be discussed later in the case study, this reaction system is composed of a first-order
140 decay and a parallel second order coupling reaction [37].

141 2.1.3. Grid independence

142 From numerical perspective, compartmental model is an upwind discretization of mass balance
143 equation with finite volume method. Underlying this discretization scheme lies the assumption of
144 homogeneity inside each control volume. Therefore, compartmental model would exhibit higher
145 diffusivity than the true medium. The deviation caused by compartmentalization depends on the
146 system being modelled and the type of discretization that is used.

147 One heuristic rule is that with higher resolution grid, the discretized model should behave more
148 like the continuous case. However, with increasing resolution, the complexity of the model also
149 increases, which leads to higher computational expenses. Moreover, decreasing grid size would lead
150 to a decreasing Péclet number, which would undermine the assumption of ignoring diffusion mass
151 transfer. Therefore, a grid independence analysis should be conducted to find the optimal grid
152 density to map the CFD data to compartmental model.

153 In this work the grid independence test is performed in two steps. First the Damköhler number
154 (Da) and Péclet number (Pe) are analyzed, as suggested in Eq.7 and Eq.8, which are critical to justify
155 the compartmentalization of model discussed in subsection 2.1.2.

156

$$Da = \frac{k_1 C_A + k_2 C_b C_A}{u C_A / L} < 1, \quad (7)$$

$$Pe = \frac{Lu}{D} > 1, \quad (8)$$

157 This analysis determines the lower and upper bounds of length scale for the compartments,
158 which could serve as a starting point for the grid independence test. Then the initial choice of length
159 scale is improved in an iterative manner. Simulations based on compartmental models with
160 decreasing length scale are tested. When the simulation results are no longer changing with the
161 increasing grid density, the model resolution can be considered as sufficient.

162 It should be mentioned that the optimal grid density depends on reaction kinetics. If the time
163 constant of chemical reactions is significantly larger than that of mixing, this process could be
164 considered mixing-insensitive and perfect mixing assumption could be adopted without harming
165 model precision. By contrast, for fast reaction, the deviation caused by perfect-mixing assumption
166 could be significant, which requires higher resolution. If the characteristic time scale of reaction is
167 orders of magnitude less than micro-mixing, which is in the order of 10^{-3} s [15], micro-mixing would
168 dominate chemical reaction. As a result, the rate law of chemical reaction should be replaced with
169 micro-mixing models. Although for different reaction kinetics we can use the same steady state
170 solution from CFD, if new reaction kinetics are used, grid independence test should be conducted
171 with the updated model.

172

173

174

175 2.2. Surrogate-based optimization

176 2.2.1. A brief review of surrogate-based optimization

177 Surrogate-based optimization have been the focus of interest in the derivative-free optimization
 178 literature. Commonly seen in science and engineering studies are complex computer simulations and
 179 experiments conducted to gain understanding of systems. As a result, for these problems derivative
 180 information is either unavailable or prohibitively hard to get, making it impossible to implement
 181 deterministic optimization methods efficiently [38]. Therefore, there is a high interest in developing
 182 methods to handle the optimization problems where limited or noisy information is available[39].

183 Surrogate-based optimization use surrogate models, which are simpler models that can mimic
 184 complex phenomenon, to guide the search in derivative-free optimization problems. Since surrogate
 185 models are computationally less demanding, surrogate-based optimization is a good compromise
 186 between describing the complex process and remaining computationally feasible. It has been
 187 demonstrated that surrogate-based optimization displays superior performance for derivative-free
 188 optimization problems [40]. Most popular surrogate models implemented for optimization methods
 189 are radial basis function (RBF) [41-45] and Kriging [46-50], due to their capability to provide
 190 prediction uncertainty. Artificial neural networks (ANN) have excellent fitting characteristics with
 191 low complexity, therefore implementations of ANN for surrogate optimization is popular for various
 192 engineering applications [51-54].

193 Surrogate optimization works in an iterative manner. In the initial step, several sampling point
 194 are chosen, and an initial surrogate model is built based on function evaluation at those sampled
 195 points. Then new sampling points are determined by evaluating the surrogate model. At new
 196 sampling point, the original model is evaluated and the surrogate model is updated. This process is
 197 conducted iteratively until a stopping criterion is met, and the best design point is chosen. In this
 198 work, the mixed-integer optimization problem is solved with surrogate optimization based on the
 199 work of Müller[55].

200 2.2.2. Problem formulation

201 In this work, the location and rate of feeding are optimized to improve reaction selectivity. Due
 202 to the perfect mixing assumption of control volumes, feeding location is represented by the index of
 203 compartment it resides at. It's worth noting that while the feeding location should be fixed
 204 throughout the process, the feeding rate could change dynamically. Therefore, by taking advantage
 205 of the extra degree of freedom through adopting a changing feeding rate, reaction selectivity could
 206 be further improved comparing to a fixed rate feeding, as will be discussed in subsection 4.2.
 207 Dynamic profile of feeding rate is defined by splitting the whole process time into N_s discrete feeding
 208 stages. Feeding rate is kept constant in each stage, but different feeding rate are employed for
 209 different stages. Each feeding stage i is specified by its duration t_i and the adopted feeding rate f_i ,
 210 which are not defined a priori, instead they are determined by solving an optimization problem.

211 In order to solve for the optimal operating policy, reaction selectivity should be quantified based
 212 on analyzing product distribution. The most intuitive definition is by segregation index, which is
 213 based on the ratio of raw material consumed by the desired product to the total raw materials
 214 injected. This method was widely adopted in previous work[2, 56, 57], where the influence of feeding
 215 rate was not investigated. However, adopting segregation index as an objective function in this work
 216 could lead to trivial solutions, due to the fact that feeding rate usually contributes monotonically to
 217 product ratio. Without considering the economics of the process, solely focusing on the product ratio
 218 would lead to unsatisfactory process design. Thus, it is recommended to use revenue as a way to
 219 capture and optimize reaction selectivity. To maximize revenue of chemical processes, the
 220 optimization problem is defined as followed.

221
 222
 223

$$\text{Maximize}_{n,t_i,f_i} (\sum P_{RYR} - \sum P_{AYA}), \quad (9)$$

224 Subject to:

$$[y_R, y_A] = \varphi(n, t_1, f_1, t_2, f_2, \dots, t_{N_p}, f_{N_p}), \quad (10)$$

$$\sum t_i = T, \forall i = 1, \dots, N_p, \quad (11)$$

$$t_i, f_i \geq 0, \forall i = 1, \dots, N_p, \quad (12)$$

$$n \in [0, N_c], \quad (13)$$

225 where P_R denotes the price of desired product R while y_R denotes its yield. P_A represents the unit
 226 cost of raw material A and its consumption is denoted as y_A . Both y_R and y_A are calculated through
 227 the simulation φ based on the compartmental model. Addition point n and addition rate profile
 228 which is defined by $t_1, f_1, t_2, f_2, \dots, t_{N_p}, f_{N_p}$ are parameters of this simulation. The first set of constraints
 229 describe the simulation based on the compartmental model. The second constraint represents that
 230 the total time span of all stages is pre-defined as T .

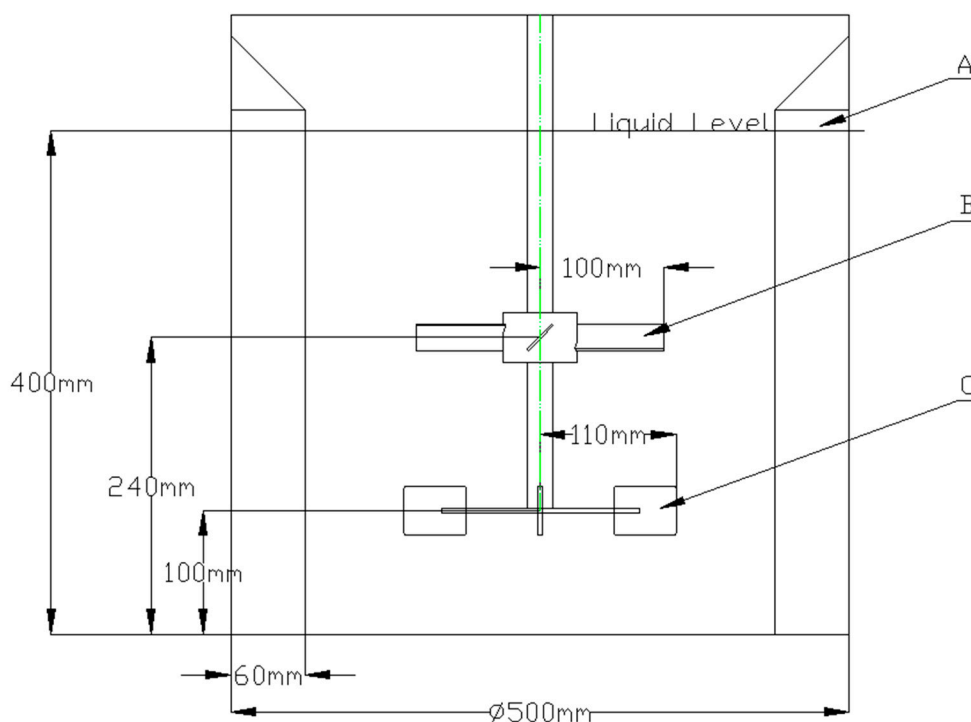
231 Notice that the number of stages is introduced as a parameter instead of decision variable. This
 232 is based on the difficulty of penalizing the monotonic increase of the number of stages. By allowing
 233 extra degrees of freedom, an increasing number of stages is always preferred. Reaction selectivity
 234 would always benefit from higher degree of freedom provided by the increasing N_p , unless
 235 computational expense of solving this optimization problem is taken into consideration. However,
 236 this is beyond the scope of this paper. Also, the duration of process T is defined as a parameter, which
 237 corresponds to the scheduling of different processes. It is recommended to define T similar to the
 238 timescale of mixing in mixing controlled processes to maximize time efficiency of reactors.

239 3. Case Study

240 In this section, a case study of a semi-batch process inside a dual-impeller stirred tank reactor is
 241 studied. The duration of the whole process is 150 seconds, in which the reagents feeding process is
 242 analyzed and optimized. A well-known pair of competitive reactions [37] is introduced to study the
 243 influence of mixing on reaction selectivity. The overall objective for the optimization problem is to
 244 maximize process productivity, which is defined as the revenue from selling the products minus the
 245 total cost of raw materials injected. In this case study, process designed according to CFD-based
 246 compartmental model and perfect-mixing model are compared to illustrate the effectiveness of this
 247 methodology. Furthermore, constant feeding rate design is compared with time-varying feeding rate
 248 to demonstrate that this framework can further improve reaction selectivity by enabling dynamic
 249 design.

250 3.1. Reactor setup

251 This study was carried out in a 74L baffled stirred vessel agitated with a Rushton impeller and
 252 a pitched blade turbine, as illustrated in Figure 1. The diameter of the vessel is $D=0.5\text{m}$, and the liquid
 253 level is $H=0.4\text{m}$ from the bottom of the vessel. The Rushton impeller is assembled $T=0.14\text{m}$ below the
 254 pitched blade turbine, whose blade angle is 45° . The agitation system is operated at 12rpm
 255 anticlockwise, which drives fluid downwards from the pitched blade turbine to the Rushton impeller.



256

257 **Figure 1.** Geometrical dimension of the two-impeller stirred tank. Where (A) stands for the baffles,
 258 (B) represents the pitched blade impeller and (C) denotes the Rushton impeller.

259 3.2. Chemical kinetics

260 To study the influence of mixing on reaction selectivity, a well-documented pair of parallel
 261 competitive Bourne reactions is integrated. This reaction system is composed of a first-order decay
 262 and a parallel second order coupling, where A is a diazonium salt (diazotized 2-chloro-4-nitroaniline)
 263 and B is pyrazolone (4-sulphophenyl-3-carboxypyrazol-5-one). R denotes the desirable product
 264 which is a dyestuff, and S is the unwanted product of decomposition. The rate constants at 40°C are
 265 $k_1=10^{-3}\text{s}^{-1}$ and $k_2=7000\text{m}^3\text{ kmol}^{-1}\text{ s}^{-1}$ at a PH=6.6[37]. Both reactants are dissolved in aqueous solution.



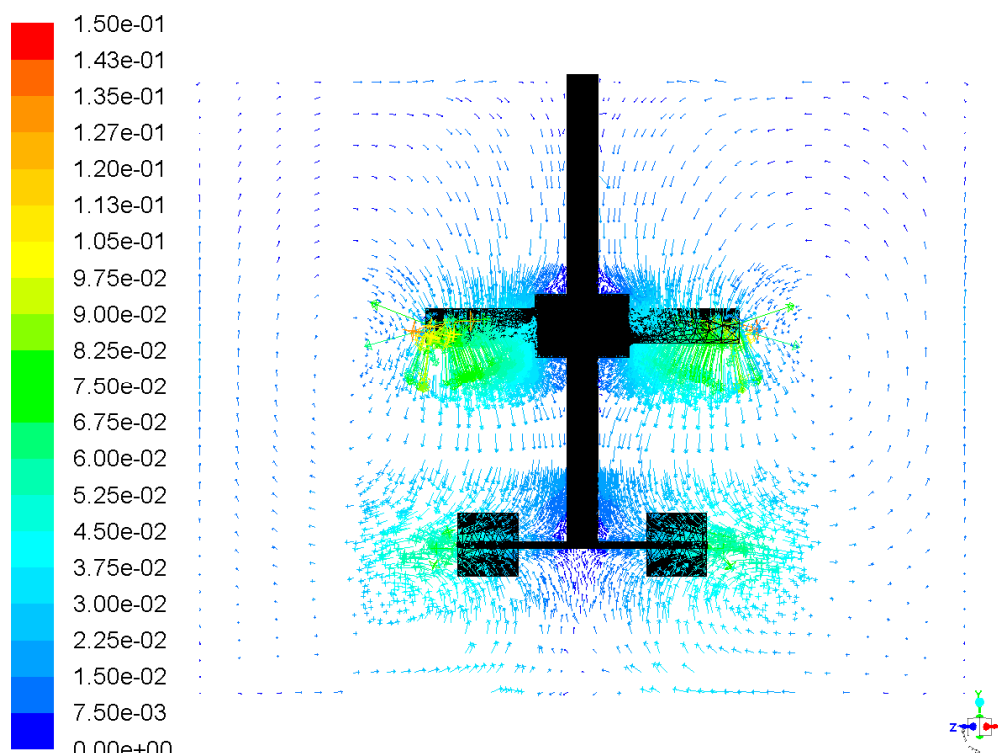
268 The vessel is initially charged with pyrazolone solution with a concentration of $1 \times 10^{-3}\text{M}$.
 269 diazonium solution is added into the stirred tank in a semi-batch manner, the concentration of which
 270 is $7.4 \times 10^{-1}\text{M}$.

271 In this reaction system, the advantage of defining objective function in the form of productivity
 272 is pronounced. Considering that the desired reaction happens faster than side reactions, infinitely
 273 slow feeding would always be preferred if we want to maximize the ratio between desired product
 274 and side product. Based the time scale of mixing, the duration of process is set as 150s.

273 3.3. Flow field simulation

274 CFD simulation is adopted to solve for velocity field inside this reactor based on the physical
 275 property of the solvent. Although Pyrazolone solution is fed in a semi-batch manner into the stirred
 276 tank, the influence of the feeding pipe over the flow pattern is ignored. Since the flow rate of injection
 277 pipe is 10^2 order smaller than that of the bulk flow inside the reactor, influence of reagent injection
 278 over the flow pattern is ignored.

279 A steady state CFD simulation is conducted with the commercial code of Fluent 16.0. The
280 Reynolds-Averaged-Navier-Stocks (RANS) equation was numerically solved with multi-reference
281 frame (MRF) method. To close the equations, k-epsilon turbulence model with standard wall
282 functions was adopted. The velocity field is shown in Figure 2.



283

284 **Figure 2.** Simulated vector plot of velocity field inside the stirred tank (m/s)

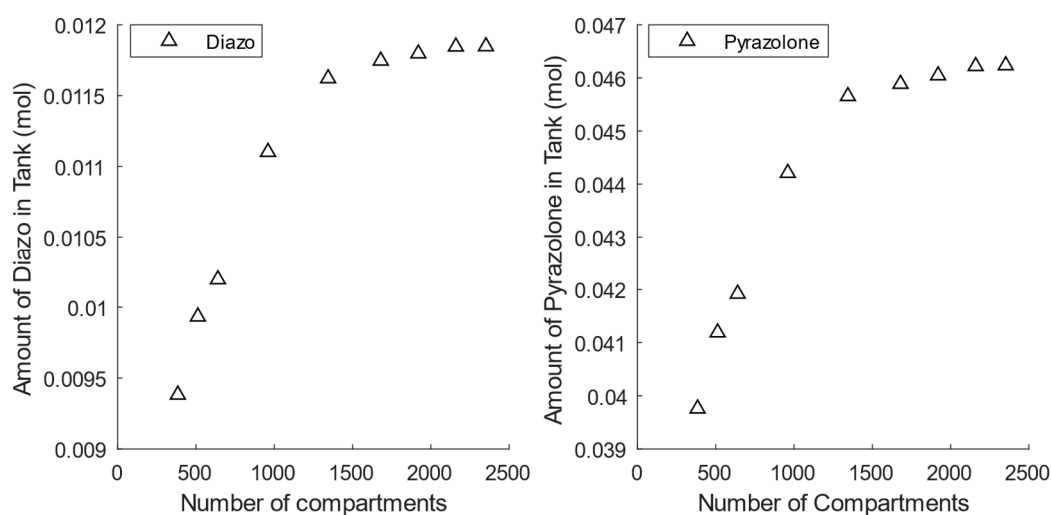
285 3.4. Compartmental modeling and grid independence test

286 To develop compartmental models from steady state CFD simulation, computational cells
287 extracted from CFD are aggregated based on a predefined grid. The grid is defined by evenly
288 dividing the reactor in radial, axial and angular directions. The grid density of each direction is
289 determined based on the grid sensitivity test proposed in subsection 2.1.3.

290 To justify the perfect-mixing assumptions in each compartment, local Damköhler number (Da)
291 is analyzed. As suggested Figure 2, the bulk velocity inside the stirred tank is in the order of 10^{-2} m/s.
292 Based on Eq.7, the upper bound of length scale in each compartment should be 1m. Furthermore, to
293 justify neglecting diffusive mass transfer, Péclet number (Pe) is analyzed according to Eq.8. Since
294 diffusion coefficient in aqueous solutions are in the order of 10^{-9} m²/s, the lower bound of
295 compartment length scale is 10^{-7} m. It can be concluded that since in single phase turbulent flow
296 convective mass transfer rate is usually several orders of magnitude higher than that of diffusion,
297 compartmental model can be safely adopted in most single phase stirred tank reactors.

298 Starting from the upper bound indicated by the analysis of Damköhler number, length scale of
299 the compartments is decreased to test the optimal grid density as discussed in section 2.1.3. In this
300 work, grid independence test is performed by simulating the injection of diazonium at the top free
301 surface of liquid near the wall. Considering that the injection should be fast enough to show mixing
302 effect, but not excessively fast so that the pyrazolone is instantly depleted and the mixing-sensitive
303 coupling is dominated by the decaying, the feeding rate of diazonium solution is set as 0.5mL/s,
304 scaled from the work of Nienow [37]. The distribution of different chemical species at the end of
305 process is predicted and monitored. The total number of compartments used for the grid sensitivity
306 test varied from 384 ($8 \times 8 \times 6$: axial \times radial \times angular) to 2352 ($12 \times 14 \times 14$). The predicted amount of
307 chemical species varies with the number of compartments and approaches asymptotic values as
308 shown in Figure 3. In good agreement with the scaling analysis, convergence is achieved with

309 1920(12×16×10) compartments for all species, which corresponds to $Da < 0.1$. For fast model
 310 development, Damköhler number can serve as an efficient criterion for defining grids [31]. Further
 311 results presented in this paper are based on this discretization scheme.



312

313 **Figure 3.** Convergence of predicted (a) Diazonium and (b) Pyrazolone distribution with number of
 314 compartments

315 3.5. Optimization and results

316 The overall objective for the optimization problem is to maximize process productivity, which
 317 is defined based on the price of different materials. In this case study the price of desired product is
 318 assumed to be ten times as much as the price of diazonium, which is 10\$/mol. The prices have
 319 profound influence on the optimal operating policy. Feeding points are defined with 3 integer
 320 variables, representing the corresponding radial, axial and angular index.

321 The optimization algorithm is first solved for the optimal static operating condition in which
 322 reagent is injected in a constant rate. To further improve the process productivity, dynamic operating
 323 conditions where the feeding rate changes dynamically are studied and optimized. Dynamic policies
 324 comprised of 2 and 3 feeding stages are discussed. Furthermore, by optimizing process design with
 325 perfect-mixing assumption, traditional design is compared with this proposed methodology.

326 3.5.1. Optimal location of feeding

327 In this section, the influence of feeding location on mixing and reaction selectivity is studied.
 328 Two operating conditions with different feeding locations are compared; one is at the bottom corner
 329 of the reactor while the other one is at the tip of Rushton impeller. The feeding rate (1mL/s) is kept
 330 constant throughout the simulation. In Figure 4 the yield trajectories of desired product are displayed
 331 when different feeding locations are adopted. Considering that stronger convective flow presents
 332 near impellers, in industry the injection point is usually placed in that region. Consistent with this
 333 empirical rule, this simulation suggests that feeding at the corner of the reactor significantly hindered
 334 the progress of reaction.

335 **Table 1.** Comparison of optimal feeding location for (a) constant rate feeding (b) two-stage dynamic
 336 feeding policy and (c) three-stage feeding policy

Reagent Injection Policy	Optimal Injection Location	
	Height(m)	Radial Position(m)
Constant Rate Feeding	0.1-0.13	0.22-0.25
Two-stage Dynamic Feeding	0.1-0.13	0.22-0.25
Three-stage Dynamic Feeding	0.1-0.13	0.22-0.25

337

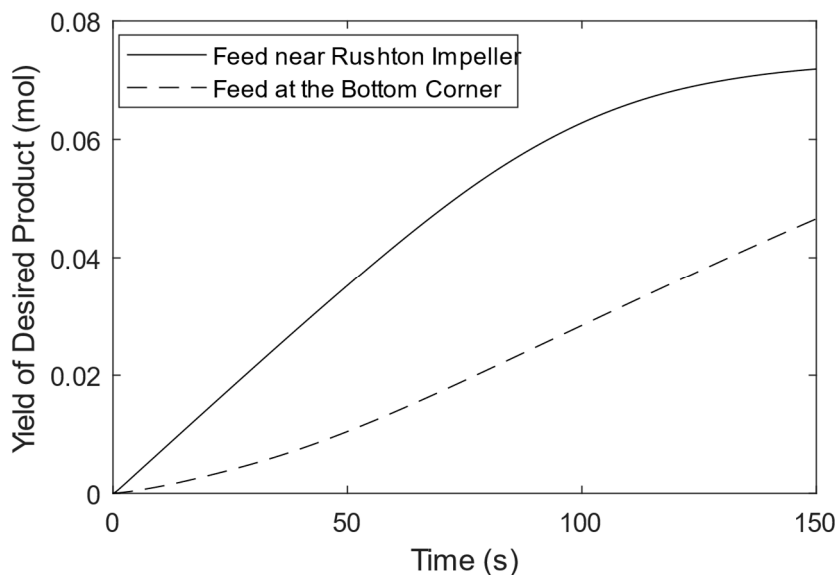
338

339

340

341

The location for feeding is then numerically optimized with the proposed compartmental model. As suggested in Table 1, it was found that irrespective of the number of stages, the maximum productivity is reached when reagents are injected at the tip of Rushton impeller, which suggests a higher mixing efficiency.



342

343

344

Figure 4. Simulated yield of the desired product when addition location is (a) at the bottom corner (b) near Rushton impeller

345

3.5.2. Optimal rate of feeding

346

347

348

349

350

The optimal feeding rate profiles determined for different reagent injection policies are illustrated in Figure 5. It can be concluded that the proposed methodology favors a decreasing feeding rate profile, which leads to an increased process productivity. The reason behind this productivity boost is studied through process dynamics. As illustrated in Table 2, approximately 4% increase in process productivity is achieved by implementing a more dynamic operation.

351

352

Table 2. Comparison of optimal process productivity when (a) constant rate feeding (b) two-stage dynamic feeding policy and (c) three-stage feeding policy are adopted

Reagent Injection Policy	Optimal Process Productivity (\$)
Constant Rate Feeding	6162.90
Two-stage Dynamic Feeding	6410.43
Three-stage Dynamic Feeding	6411.76

353

354

355

356

357

358

359

Simulated trajectories of chemical species when different injection policies are employed is illustrated in Figure 6. It is suggested that through employing dynamic policies, the yield of desired product is not significantly enhanced (Figure 6(c)), which can be explained by the way we formulate this problem. Since the price of the desired product is 10 times as high as the price of diazonium, through the effort to maximize the overall profit, sufficient diazonium is fed to exhaust pyrazolone, which lead to similar yield of the product.

360

361

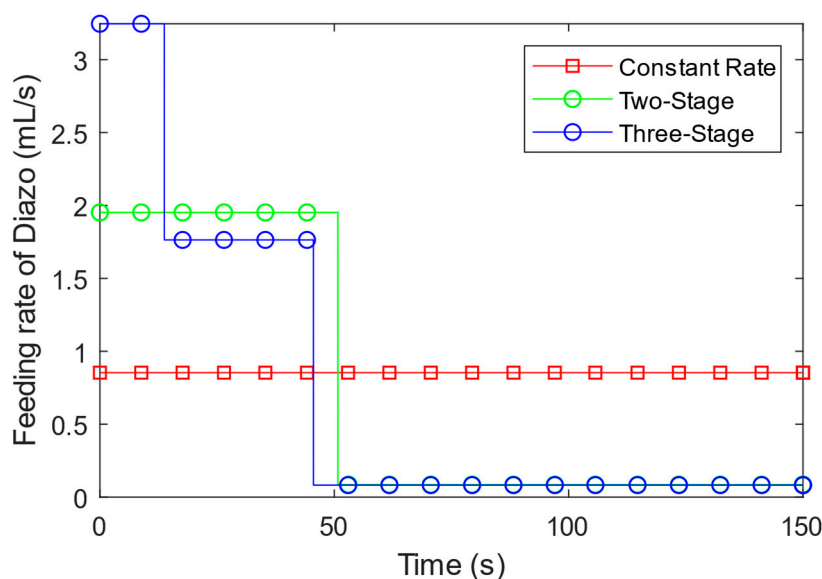
362

363

364

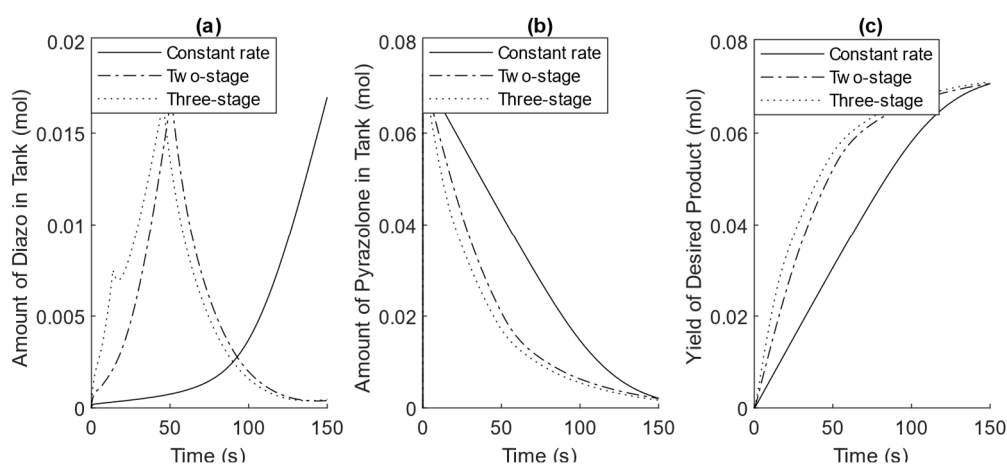
365

Nevertheless, dynamic feeding rate can improve process productivity through reducing the waste of raw material. As suggested in Figure 6(a), considerable amount of diazonium is wasted if constant rate feeding policy is adopted. When reactant is fed at a constant rate, with the consumption of pyrazolone, diazonium would inevitably accumulate faster, which lead to material waste that compromises economic performance. By adjusting feeding rate as pyrazolone is deleted, maximum process profit can be achieved.



366
367
368

Figure 5. Optimal feeding rate profile solved for (a) Constant rate (b) Two-stage (c) Three-stage reagent injection policies



369
370
371

Figure 6. Simulated trajectories of (a) Diazo (b) Pyrazolone and (c) Desired product when optimal feeding policies solved with different number of stages are employed

372 3.5.3. Traditional process design with perfect-mixing assumptions

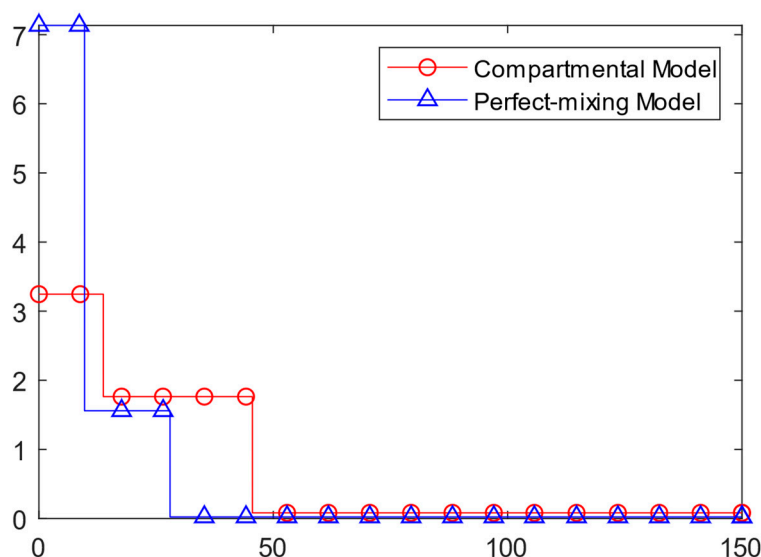
373 To illustrate the improvement of reaction selectivity by implementing this proposed
374 methodology, perfect-mixing model is studied and compared with compartmental model. The same
375 optimization algorithm is applied to the process dynamics model developed under perfect mixing
376 assumption. Specifically, in this section, three-stage dynamic feeding rate is considered. Table 3
377 shows the simulated process productivity when different methodologies are employed. It can be
378 concluded that by capturing the heterogeneity with CFD-based compartmental model, significant
379 improvement to process productivity could be achieved. The reason behind this productivity boost
380 is studied through process dynamics, as shown in Figure 7 and Figure 8.

381
382

Table 3. Comparison between optimal operating conditions solved with perfect mixing model and the proposed methodology

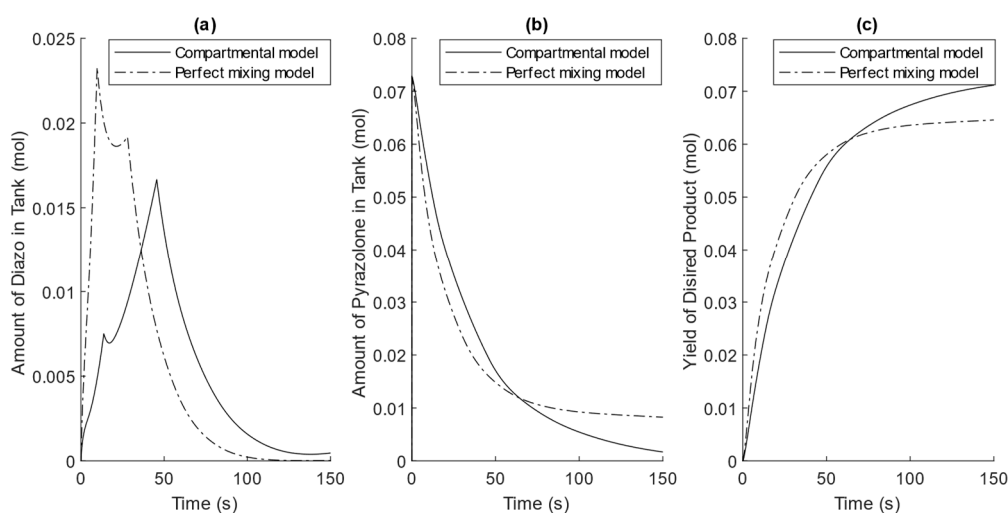
Methodology	Simulated Process Productivity (\$)
Perfect-mixing Model	6162.90
CFD-based Compartmental Model	6410.43

383 Optimal feeding rate profiles determined with different methodologies are illustrated in Figure
 384 7. It is suggested that process design based on perfect-mixing assumption would lead to faster feeding
 385 at earlier period of process. Therefore, a high quantity of diazonium is accumulated in the earlier
 386 stage of process (Figure 8(a)). As a result, the undesired decomposition of diazonium is accelerated,
 387 which compromise reaction selectivity (Figure 8(d)). Moreover, without considering the insufficient
 388 consumption of pyrazolone due to imperfect mixing, the overall yield of desired product is hindered,
 389 which further reduced product productivity.



390

391 **Figure 7.** Optimal feeding rate profile solved with (a) CFD-based compartmental model and (b)
 392 perfect mixing model



393

394 **Figure 8.** Simulated trajectories of (a) Diazonium (b) Pyrazolone (c) Desired product and (d)
 395 undesired product when different methodologies are employed

396 4. Discussion

397 Mixing in turbulent flow can significantly influence reaction selectivity, therefore systematic
 398 analysis of mass transfer inside reactors is crucial for process design. Despite the increasing
 399 computational power available for gaining understanding of the mixing process, in-silico process
 400 design can still be inefficient in time and cost. In this proposed framework, by replacing repetitive
 401 dynamic CFD simulation with compartmental model, process design can be conducted in a timely
 402 and economically more efficient manner. Moreover, in this work surrogate-based optimization is

403 implemented to numerically optimize process productivity. Comparing to genetic algorithm, which
 404 is most widely adopted in engineering design, surrogate-based method requires less simulations to
 405 find the optimal process design. As a result, the overall time efficiency can be significantly improved.

406 From the case study in section 3, it can be concluded from Table 4 that by implementing CFD-
 407 based compartmental modeling, significant time saving could be achieved. Single simulations were
 408 performed to determine the computational effort for one design evaluation. The hardware used is a
 409 4-cores Intel Xeon E5 V3 workstation. In active pharmaceutical ingredient (API) plant design where
 410 a large number of simulations are conducted, computational expense could be reduced from weeks
 411 to hours through the implementation of the proposed methodology. Moreover, considering that CFD
 412 is not freely available and requires special know-how, by cutting back dynamics CFD simulations,
 413 implementing compartmental modeling is economically beneficial. This approach has shown a good
 414 potential to characterize mixing in all the reactors in an API plant.

415 **Table 4.** Comparing computational expense between the proposed methodology and direct CFD
 416 simulation

Methodology	Computational Expense for one Simulation (s)
Dynamic CFD simulation	10 ⁴
CFD-based Compartmental Model	70

417 Despite the reduced model complexity, in this work the grid density is determined so that
 418 inhomogeneity inside reactor is sufficiently captured. Comparing to traditional process design
 419 strategies which are based on perfect-mixing assumption, better reaction selectivity could be
 420 achieved through compartmental model. As has been discussed in subsection 3.5.3, by replacing
 421 traditional process design strategy with this proposed compartmental model, more than 10% increase
 422 in process profit has been achieved (Table 3).
 423

424 **Table 5.** Comparison between optimal operating conditions solved with perfect mixing model and
 425 the proposed methodology

Methodology	Simulated Process Productivity (\$)
Perfect-mixing Model	5713.18
Compartmental Model (constant rate)	6126.90
Compartmental Model (dynamic rate)	6411.76

426 Furthermore, this proposed framework allows the design of dynamic operations. As illustrated
 427 in subsection 3.5.2, by adapting feeding rate in time to account for the depletion of raw materials,
 428 material waste can be substantially reduced, which in turn leads to improved process productivity.
 429 Considering that for complex reaction networks commonly encountered in organic synthesis, process
 430 dynamics could be very complicated. By enabling the design of dynamic operations to fit the evolving
 431 chemical processes, this proposed framework has exhibited a great potential of productivity
 432 improvement.
 433

434 5. Summary

435 In this work, a methodology to improve reaction selectivity by optimizing process operation is
 436 proposed. Detailed CFD simulation is incorporated with computationally inexpensive
 437 compartmental model and reaction kinetics, yielding a good compromise between accuracy and
 438 complexity. An efficient surrogate optimization algorithm is integrated, making this framework
 439 promising for rapid process design. As suggested in the case study, by directly accounting for the
 440 product distribution from Bourne reactions, this proposed methodology can successfully improve
 441 process design and optimize reaction selectivity. Furthermore, the proposed methodology allows for
 442 dynamic process operation design, which has shown a great potential of further productivity
 443 improvement. This methodology can be applied not only to stirred tank reactors, but also to

444 completely different reactors including flow reactors and crystallizers. Finally, the developed
445 simplification of complex transport model has the potential for advanced process monitoring and
446 control for reactors with limited instrumentation, such as single-use bioreactors and fermenters.

447 **Author Contributions:** Under supervision of M.I. and S.K., S.Y. was responsible for development of research
448 methodology and optimization framework, model development, optimization and analysis of the results. P.F.
449 contributed in model development.

450 **Funding:** This research received no external funding.

451 **Acknowledgments:** The authors gratefully acknowledge financial support from Gilead Science Inc. We also
452 appreciate the discussions and technical inputs from Chiajen Lai of Gilead Science Inc.

453 **Conflicts of Interest:** The authors declare no conflicts of interest.

454 References

- 455 1. Plutschack, M.B., et al., The Hitchhiker's Guide to Flow Chemistry(II). *Chem. Rev.*, **2017**. 117(18): p. 11796-
456 11893.
- 457 2. Gobert, S.R.L., et al., Characterization of Milli- and Microflow Reactors: Mixing Efficiency and Residence
458 Time Distribution. *Org. Process Res. Dev.*, **2017**. 21(4): p. 531-542.
- 459 3. Fogler, H.S., *Essentials of chemical reaction engineering*. 2010: Pearson Education.
- 460 4. Gresch, M., et al., Compartmental Models for Continuous Flow Reactors Derived from CFD Simulations.
461 *Environ. Sci. Technol.*, **2009**. 43(7): p. 2381-2387.
- 462 5. Nienow, A.W., On impeller circulation and mixing effectiveness in the turbulent flow regime. *Chem. Eng.*
463 *Sci.*, **1997**. 52(15): p. 2557-2565.
- 464 6. Rosseburg, A., et al., Hydrodynamic inhomogeneities in large scale stirred tanks - Influence on mixing
465 time. *Chem. Eng. Sci.*, **2018**. 188: p. 208-220.
- 466 7. Levesque, F., et al., Advancing Flow Chemistry Portability: A Simplified Approach to Scaling Up Flow
467 Chemistry. *Org. Process Res. Dev.*, **2018**. 22(8): p. 1015-1021.
- 468 8. Aubin, J.; Ferrando, M.; Jiricny, V., Current methods for characterising mixing and flow in microchannels.
469 *Chem. Eng. Sci.*, **2010**. 65(6): p. 2065-2093.
- 470 9. Commenge, J.M.; Falk, L., Villermaux-Dushman protocol for experimental characterization of micromixers.
471 *Chem. Eng. Process.*, **2011**. 50(10): p. 979-990.
- 472 10. Reckamp, J.M., et al., Mixing Performance Evaluation for Commercially Available Micromixers Using
473 Villermaux-Dushman Reaction Scheme with the Interaction by Exchange with the Mean Model. *Org.*
474 *Process Res. Dev.*, **2017**. 21(6): p. 816-820.
- 475 11. Bourne, J.R.; Kozicki, F.; Rys, P., Mixing and fast chemical reaction—I: Test reactions to determine
476 segregation. *Chem. Eng. Sci.*, **1981**. 36(10): p. 1643-1648.
- 477 12. Bourne, J.R., Mixing and the selectivity of chemical reactions. *Org. Process Res. Dev.*, **2003**. 7(4): p. 471-508.
- 478 13. Bourne, J.R.; Yu, S.Y., Investigation of micromixing in stirred tank reactors using parallel reactions. *Ind.*
479 *Eng. Chem. Res.*, **1994**. 33(1): p. 41-55.
- 480 14. Fournier, M.C.; Falk, L.; Villermaux, J., A new parallel competing reaction system for assessing
481 micromixing efficiency—Experimental approach. *Chem. Eng. Sci.*, **1996**. 51(22): p. 5053-5064.
- 482 15. Cheng, D., et al., Numerical simulation of macro-mixing in liquid-liquid stirred tanks. *Chem. Eng. Sci.*, **2013**.
483 101: p. 272-282.
- 484 16. Liu, L.; Barigou, M., Experimentally Validated Computational Fluid Dynamics Simulations of
485 Multicomponent Hydrodynamics and Phase Distribution in Agitated High Solid Fraction Binary
486 Suspensions. *Ind. Eng. Chem. Res.*, **2014**. 53(2): p. 895-908.
- 487 17. Warmeling, H.; Behr, A.; Vorholt, A.J., Jet loop reactors as a versatile reactor set up - Intensifying catalytic
488 reactions: A review. *Chem. Eng. Sci.*, **2016**. 149: p. 229-248.
- 489 18. Reinecke, S.F., et al., Macro-mixing characterisation of a stirred model fermenter of non-Newtonian liquid
490 by flow following sensor particles and ERT. *Chem. Eng. Res. Des.*, **2017**. 118: p. 1-11.
- 491 19. Varela, S., et al., Numerical and experimental modelization of the two-phase mixing in a small scale stirred
492 vessel. *J. Ind. Eng. Chem.*, **2018**. 60: p. 286-296.
- 493 20. Farzan, P.; Ierapetritou, M.G., Integrated modeling to capture the interaction of physiology and fluid
494 dynamics in biopharmaceutical bioreactors. *Comput. Chem. Eng.*, **2017**. 97: p. 271-282.

- 495 21. Lladó Maldonado S., et al., Multiphase microreactors with intensification of oxygen mass transfer rate and
496 mixing performance for bioprocess development. *Biochem. Eng. J.*, **2018**. 139: p. 57-67.
- 497 22. Zhan, C.J., et al., Study of hydrodynamics in wave bioreactors by computational fluid dynamics reveals a
498 resonance phenomenon. *Chem. Eng. Sci.*, **2019**. 193: p. 53-65.
- 499 23. Smith, J.D., et al., CFD-Based Optimization of a Flooded Bed Algae Bioreactor. *Ind. Eng. Chem. Res.*, **2013**.
500 52(22): p. 7181-7188.
- 501 24. Uebel, K., et al., CFD-based multi-objective optimization of a quench reactor design. *Fuel Process. Technol.*,
502 **2016**. 149: p. 290-304.
- 503 25. Rossgger, P.; Richter, A., Performance of different optimization concepts for reactive flow systems based on
504 combined CFD and response surface methods. *Comput. Chem. Eng.*, **2018**. 108: p. 232-239.
- 505 26. Park, S., et al., Multi-objective Bayesian optimization of chemical reactor design using computational fluid
506 dynamics. *Comput. Chem. Eng.*, **2018**. 119: p. 25-37.
- 507 27. Bezzo, F.; Macchietto, S.; Pantelides, C.C., A general methodology for hybrid multizonal/CFD models.
508 *Comput. Chem. Eng.*, **2004**. 28(4): p. 501-511.
- 509 28. Nauha, E.K., et al., Compartmental modeling of large stirred tank bioreactors with high gas volume
510 fractions. *Chem. Eng. J.*, **2018**. 334: p. 2319-2334.
- 511 29. Nørregaard, A., et al., Hypothesis-driven compartment model for stirred bioreactors utilizing
512 computational fluid dynamics and multiple pH sensors. *Chem. Eng. J.*, **2019**. 356: p. 161-169.
- 513 30. Boltersdorf, U.; Deerberg, G.; Schlüter, S., Computational study of the effects of process parameters on the
514 product distribution for mixing sensitive reactions and on distribution of gas in stirred tank reactors. *Recent
515 research developments in chemical engineering*, **2000**: p. 15-43.
- 516 31. Guha, D., et al., CFD-based compartmental modeling of single phase stirred-tank reactors. *AIChE J.*, **2006**.
517 52(5): p. 1836-1846.
- 518 32. Zhao, W., et al., Application of the compartmental model to the gas-liquid precipitation of CO₂-Ca(OH)₂
519 aqueous system in a stirred tank. *AIChE J.*, **2017**. 63(1): p. 378-386.
- 520 33. Vrabel, P., et al., Compartment model approach: Mixing in large scale aerated reactors with multiple
521 impellers. *Chem. Eng. Res. Des.*, **1999**. 77(A4): p. 291-302.
- 522 34. Du, J.; Johansen, T.A., Integrated Multilinear Model Predictive Control of Nonlinear Systems Based on Gap
523 Metric. *Ind. Eng. Chem. Res.*, **2015**. 54(22): p. 6002-6011.
- 524 35. Srilatha, C., et al., Relation between hydrodynamics and drop size distributions in pump-mix mixer. *Chem.
525 Eng. Sci.*, **2010**. 65(11): p. 3409-3426.
- 526 36. Bezzo, F.; Macchietto, S., A general methodology for hybrid multizonal/CFD models - Part II. Automatic
527 zoning. *Comput. Chem. Eng.*, **2004**. 28(4): p. 513-525.
- 528 37. Nienow, A.W., et al., A new pair of reactions to characterize imperfect macro-mixing and partial
529 segregation in a stirred semi-batch reactor. *Chem. Eng. Sci.*, **1992**. 47(9-11): p. 2825-2830.
- 530 38. Conn, A.R.; Scheinberg, K.; Vicente, L.N., *Introduction to derivative-free optimization*. Vol. 8. 2009: Siam.
- 531 39. Boukouvala, F.; Misener, R.; Floudas, C.A., Global optimization advances in Mixed-Integer Nonlinear
532 Programming, MINLP, and Constrained Derivative-Free Optimization, CDFO. *Eur. J. Oper. Res.*, **2016**.
533 252(3): p. 701-727.
- 534 40. Bhosekar, A.; Ierapetritou, M., Advances in surrogate based modeling, feasibility analysis, and
535 optimization: A review. *Comput. Chem. Eng.*, **2018**. 108: p. 250-267.
- 536 41. Regis, R.G.; Shoemaker, C.A., Improved strategies for radial basis function methods for global
537 optimization. *J. Glob. Optim.*, **2007**. 37(1): p. 113-135.
- 538 42. Oeuvray, R.; Bierlaire, M., BOOSTERS: A derivative-free algorithm based on radial basis functions. *Int. J.
539 Model. Simul.*, **2009**. 29(1): p. 26-36.
- 540 43. Wild, S.M.; Shoemaker, C.A., Global Convergence of Radial Basis Function Trust-Region Algorithms for
541 Derivative-Free Optimization. *SIAM Rev.*, **2013**. 55(2): p. 349-371.
- 542 44. Regis, R.G.; Wild, S.M., CONORBIT: constrained optimization by radial basis function interpolation in trust
543 regions. *Optim. Method Softw.*, **2017**. 32(3): p. 552-580.
- 544 45. Wang, Z.L.; Ierapetritou, M., A novel feasibility analysis method for black-box processes using a radial
545 basis function adaptive sampling approach. *AIChE J.*, **2017**. 63(2): p. 532-550.
- 546 46. Jones, D.R.; Schonlau, M.; Welch, W.J., Efficient global optimization of expensive black-box functions. *J.
547 Glob. Optim.*, **1998**. 13(4): p. 455-492.

- 548 47. Boukouvala, F.; Ierapetritou, M.G., Derivative-free optimization for expensive constrained problems using
549 a novel expected improvement objective function. *AIChE J.*, **2014**, *60*(7): p. 2462-2474.
- 550 48. Regis, R.G., Trust regions in Kriging-based optimization with expected improvement. *Eng. Optimiz.*, **2016**,
551 *48*(6): p. 1037-1059.
- 552 49. Beykal, B., et al., Global optimization of grey-box computational systems using surrogate functions and
553 application to highly constrained oil-field operations. *Comput. Chem. Eng.*, **2018**, *114*: p. 99-110.
- 554 50. Wang, Z.L.; Ierapetritou, M., Constrained optimization of black-box stochastic systems using a novel
555 feasibility enhanced Kriging-based method. *Comput. Chem. Eng.*, **2018**, *118*: p. 210-223.
- 556 51. Fernandes, F.A.N., Optimization of Fischer-Tropsch synthesis using neural networks. *Chem. Eng. Technol.*,
557 **2006**, *29*(4): p. 449-453.
- 558 52. Henaio, C.A.; Maravelias, C.T., Surrogate-Based Superstructure Optimization Framework. *AIChE J.*, **2011**,
559 *57*(5): p. 1216-1232.
- 560 53. Brar, L.S.; Elsayed, K., Analysis and optimization of cyclone separators with eccentric vortex finders using
561 large eddy simulation and artificial neural network. *Sep. Purif. Technol.*, **2018**, *207*: p. 269-283.
- 562 54. Sen, O., et al., Evaluation of multifidelity surrogate modeling techniques to construct closure laws for drag
563 in shock-particle interactions. *J. Comput. Phys.*, **2018**, *371*: p. 434-451.
- 564 55. Müller, J., MISO: mixed-integer surrogate optimization framework. *Optim. Eng.*, **2015**, *17*(1): p. 177-203.
- 565 56. Zhang, W.P., et al., Investigation of Mixing Performance in Passive Micromixers. *Ind. Eng. Chem. Res.*, **2016**,
566 *55*(38): p. 10036-10043.
- 567 Lin, X.Y., et al., Liquid-liquid mixing enhancement rules by microbubbles in three typical micro-mixers.
568 *Chem. Eng. Sci.*, **2015**, *127*: p. 60-71.